### Title

An approach to zwitterionic peptide design for colorimetric detection of the Southampton norovirus SV3CP protease.




### Journal

Analyst, 148(18)



### Authors

Yeung, Justin

Jin, Zhicheng

Ling, Chuxuan

et al.



### Publication Date

2023-09-11

### DOI

10.1039/d3an00873h

Peer reviewed

HHS Public Access

Author manuscript

*Analyst*. Author manuscript; available in PMC 2024 September 11.

Published in final edited form as:

*Analyst*. ; 148(18): 4504–4512. doi:10.1039/d3an00873h.

# An approach to zwitterionic peptide design for colorimetric detection of the Southampton norovirus SV3CP protease†

**Justin Yeung**[a], **Zhicheng Jin**[b], **Chuxuan Ling**[b], **Maurice Retout**[b], **Elany Barbosa da Silva**[c], **Manan Damani**[c], **Yu-Ci Chang**[d], **Wonjun Yim**[d], **Anthony J. O'Donoghue**[c], **Jesse V. Jokerst**[b,d,e]

[a]Department of Bioengineering, University of California San Diego, La Jolla, CA 92093, USA

[b]Department of NanoEngineering, University of California, San Diego, La Jolla, CA 92093, United States

[c]Skaggs School of Pharmacy and Pharmaceutical Sciences, University of California, San Diego, La Jolla, CA 92093, USA

[d]Materials Science and Engineering Program, University of California, San Diego, La Jolla, CA 92093, USA

[e]Department of Radiology, University of California, San Diego, La Jolla, CA 92093, USA

## Abstract

Noroviruses are highly contagious and are one of the leading causes of acute gastroenteritis worldwide. Due to a lack of effective antiviral therapies, there is a need to diagnose and surveil norovirus infections to implement quarantine protocols and prevent large outbreaks. Currently, the gold standard of diagnosis uses reverse transcription polymerase chain reaction (RT-PCR), but PCR can have limited availability. Here, we propose a combination of a tunable peptide substrate and gold nanoparticles (AuNPs) to colorimetrically detect the Southampton norovirus 3C-like protease (SV3CP), a key protease in viral replication. Careful design of the substrate employs a zwitterionic peptide with opposite charged moieties on the C- and N- termini to induce a rapid color change visible to the naked eye; thus, this color change is indicative of SV3CP activity. This work expands on existing zwitterionic peptide strategies for protease detection by systematically evaluating the effects of lysine and arginine on nanoparticle charge screening. We also determine a limit of detection for SV3CP of 28.0 nM with comparable results in external breath condensate,

†Electronic supplementary information (ESI) available: Materials, materials synthesis, dynamic range measurements, LoD measurements, enzyme–substrate characterization, probing interparticle interactions, matrix test, peptide computational folding data, confirmation of SV3CP-mediated cleavage of peptides, SV3CP LoD after 8 hours, matrix effects on colloidal stability, and fecal matter dilutions. See DOI: https://doi.org/10.1039/d3an00873h

jjokerst@ucsd.edu .

Author contributions

J. Y., Z. J., and J. V. J. designed the research. J. Y., Z. J., and C. L. designed and performed the experiments. M. R. acquired the FTIR data. J. Y. and E. B. S. determined the specificity constant. E. B. S., M. D., and A. J. O. contributed the SV3CP. J. Y., Z. J., C. L., M. R., E. B. S., Y.-C. C., W. Y., and J. V. J. analyzed and interpreted the data. J. Y. and J. V. J. wrote the manuscript. All authors critically revised the paper.

Conflicts of interest

There are no conflicts to declare.

urine, and fecal matter for 100 nM of SV3CP. The key advantage of this system is its simplicity and accessibility, thus making it an attractive tool for qualitative point-of-care diagnostics.

## Introduction

Human noroviruses (HNV) are one of the leading causes of gastrointestinal illness and are responsible for an estimated 685 million cases worldwide per year according to the Centers for Disease Control and Prevention.[1] In the United States alone, HNV is the leading cause of outbreaks from contaminated food, accounting for about 50% of food-related illness outbreaks.[2] These outbreaks are common in settings such as schools, military barracks, cruise ships, and resorts. Importantly, HNV can be transmitted from person-to-person and through surfaces contaminated by viral particles from emesis, stool, and aerosolized particles, unlike food poisoning which is from toxins (*e.g.*, those produced by the bacteria *Staphylococcus aureus*).2,3 Due to the lack of vaccines or antiviral therapies, outbreak management is reliant on diagnostic evaluation followed by quarantine. This also helps to distinguish the viral infection from other foodborne illnesses which share similar symptoms. The most common diagnostic methods are enzyme immunoassays and reverse transcription polymerase chain reaction (RT-PCR).[4,5] However, these methods are rarely available at the point of care.

Ideally, the goal is to have quick isolation and identification of infected people to prevent additional spread, which can be achieved with point of care testing. Colorimetric sensors utilizing gold nanoparticles (AuNPs) can be a cost-effective and intuitive diagnostic platform that can resolve the inherent limitations of established protocols. AuNP-based diagnostics have gathered attention regarding their use in *in vitro* diagnostics due to their distinct physical and optical properties including localized surface plasmon resonance (LSPR) and fluorescence resonance energy transfer (FRET).[6] Aggregation of these particles can induce interparticle plasmon coupling and exploit the AuNPs' ultrahigh extinction coefficient to generate a significant absorption band shift in the visible region of the electromagnetic spectrum, thus resulting in a pronounced red-to-blue color change visible to the naked eye.[6] Additionally, surface modifications of AuNPs can provide diverse functionalization options that allow for robust interfacing of the particles through electrostatic, dithiol bridging, or amphiphilic interactions to promote aggregation.[7–10]

To bridge the gap between these interparticle interactions and viral particle screening, peptides can be used as an effective probe for proteolytic detection due to their diverse and tunable functional groups found on amino acid side chains. By exploiting the critical proteolytic post-processing step within the viral protein lifecycle, custom peptide substrates can be engineered to be activated in the presence of viral proteases to induce plasmonic coupling of AuNPs and subsequently produce a pronounced color change indicative of proteolysis.[11] More specifically, the proteolytic peptide products can be tuned to aggregate the AuNPs stabilized by their repulsive electrostatic double layer *via* charge screening.[9,12] Additionally, proteolytic catalysis can have profound signal amplification as multiple substrates can be catalysed at a time. Similar approaches using AuNPs to electrostatically detect heavy metal ions in colorimetric assays have also been reported.[13] Plasmonic sensing

has also been used in detecting other proteases including thrombin, furin, trypsin, and SARS CoV-2 Mpro.[9,14–16] In principle, this approach can be generalized to other proteases by simply adjusting the cleavage recognition sequence to be suitable for molecular recognition between the target enzyme and substrate.

Here, we build on prior work for zwitterionic peptides, $(Asp)_n$-$(AA)_x$-$(Arg)_m$, which are known to induce AuNP aggregation following proteolysis by examining the effects of lysine residues in conjunction with arginine residues on AuNP charge screening (*e.g.*, $(Asp)_n(Glu)_o$-$(AA)_x$-$(Arg)_m(Lys)_p$).[6] Simultaneously, we apply the improved zwitterionic peptide design towards a novel target: SV3CP implicated in HNV. The kinetics of the AuNPs with peptides were studied, and the aggregation state was measured. We then evaluated the generalizability of this approach by applying this system to colorimetrically measure the Southampton norovirus 3C-like protease (SV3CP). SV3CP plays a key role in the processing of a 200 kDa polyprotein encoded by ORF1, which is essential to viral replication, and lacks human homologues, making it an ideal target for diagnosis.[17] The specificity of our designed substrate was examined, and the protease detection limit was determined to be 28.0 nM. Finally, the plasmonic sensing system's performance was tested in relevant biological matrices and had a notable performance in external breath condensate, urine, and 1% fecal matter. This approach can be a valuable and economical tool for HNV diagnosis.

## Results and discussion

### Rationale

Here, we use bis(*p*-sulfonatophenyl)phenylphosphine-modified AuNPs (BSPP-AuNPs) to interface with the cleavable zwitterionic peptide substrates. To obtain these particles, a ligand exchange was performed according to our previous studies, starting with citrate-AuNPs to BSPP-AuNPs.[18,19] Functionalization of AuNPs with the BSPP ligand gave the nanoparticles considerable colloidal stability relative to the native citrate particles.[7] This stability is due to the strong negative charges found in the sulfonate groups of BSPP, effective gold-phosphorous gold coordination, steric hindrance from bulky aromatic rings, and strong electrostatic double layer repulsions.[20] As a result, the BSPP-capped nanoparticles can remain colloidally stable in various media, making them suitable for use in buffers and higher salt concentrations.

Fig. 1a shows that the zwitterionic peptide mimics these salts (*e.g.*, NaCl) because it carries oppositely charged termini (*e.g.*, $(Asp)_n$ and $(Glu)_o$ *vs.* $(Arg)_m$ and $(Lys)_p$) flanking the SV3CP-specific cleavage site $(AA)_x$. With $n + o \geq m + p$ (*e.g.*, $(Asp)_n(Glu)_o$-$(AA)_x$-$(Arg)_m(Lys)_p$), the peptide substrate carries a net neutral or negative charge, minimizing its interactions with the BSPP-AuNPs due to the negatively charged sulfonate groups carried by the ligand. Upon proteolysis, the peptide is segmented into its corresponding negatively charged and positively charged fragments, thereby altering the electrophoretic properties of the substrate. The resulting positive cleavage product can then trigger the collapse of the nanoparticle suspension *via* electrostatic interactions, thus creating a color change visible to the naked eye.

### Characterization of nanoparticle ligand exchange

To validate the successful ligand exchange of the native citrate particles with the BSPP ligand, we characterized the BSPP-capped particles using dynamic light scattering (DLS) and zeta potential measurements (Table 1 and Fig. 1b). The hydrodynamic diameter (DH) and polydispersity index (PDI) show slight increases with a slight decrease of the zeta potential, characteristic of the stronger negatively charged sulfonate groups relative to the native citrate anions. These results are largely consistent with our past studies of this specific ligand exchange.[7,9] Furthermore, a Fourier transform infrared (FTIR) spectroscopy of the particles before and after the ligand exchange shows the removal of most of the native citrate and binding of the BSPP ligand onto the nanoparticle surface (Fig. 1c and d), as noted by symmetrical and asymmetrical stretching of the S–O bond from the BSPP ligand, indicating a successful ligand exchange.

### Interactions between the nanoparticles and SV3CP-cleavable peptides

As mentioned, the zwitterionic peptide design describes a net neutral charge of the intact peptide by balancing repeating units of aspartic acid (Asp, D) and arginine (Arg, R).[9] The simplicity of this design lies in solely altering the cleavage recognition site flanked by the charged amino acids when targeting new proteases. More specifically, the flanking sites consist of an N-terminal charge-shielding site made of repeating Asp units and a C-terminal aggregating site made of repeating Arg units. However, in the case of SV3CP, literature has identified a SV3CP-cleavage recognition sequence of EFQLQ↓GK, notably containing glutamic acid (Glu, E) and lysine (Lys, K).[4] Glu and Asp are structurally very similar, with Glu containing one additional methylene group in its side chain; both carry a charge of −1 at a pH of 8. The issue lies in the difference in aggregation propensity due to presence of the Lys residue, as it remains in the C-terminal region of the cleavage site and will subsequently be liberated in the positively charged aggregating site. Arg is often the preferred amino acid over Lys for giving cationic properties to peptides, as its positive charge is stabilized by several resonance forms of the guanidine side chain, giving it a p$K_a$ of 12.0 in water *versus* Lys, which has a p$K_a$ of 10.4.[21–24] Additionally, the guanidium group can facilitate interactions in three possible directions, with anionic counterparts through its three asymmetrical nitrogen atoms.[7] Previously, the positively charged fragment was optimized to include two Arg residues for charge screening BSPP-AuNPs.[9] The difference in cationic properties between Lys and Arg suggests potential differences in their ability to charge screen the nanoparticles, which will be explored later. Here, we propose an initial peptide substrate N6: DADEFQLQ↓GKAR (net charge = 0). Proteolysis by SV3CP of N6 results in the formation of two fragments: DADEFQLQ (net charge = −3) and GKAR (net charge = +2).

AuNP aggregates induced by the N6 peptide were first characterized using transmission electron microscopy (TEM) (Fig. 2a and b). In the presence of intact N6 peptide, the BSPP-AuNPs remain colloidally stable, with the nanoparticles clearly aggregating upon incubation with N6 fragments. DLS profiles of the particles incubated with intact and SV3CP-cleaved N6 peptide further support this, as shown by the nearly 50-fold increase in hydrodynamic size ($D_H$) indicative of large aggregates (Fig. 2c). To quantitatively assess the aggregation state and resulting color change of the nanoparticles, the UV/Vis spectra of the nanoparticles

was analyzed (Fig. 2d). Incubation with the N6 fragment led up to a two-fold decrease in the LSPR at 520 nm, with a seven-fold increase in absorbance in the 600–650 nm region. We then defined the ratiometric signal, $Abs_{600}/Abs_{520}$, as a metric to quantify aggregation intensity and color change.[7–10]

Next, we investigated the aggregation kinetics of the nanoparticles when incubated with increasing concentrations of N6 fragments (Fig. 2e). Here, we see that aggregation is both time- and concentration-dependent. The 10-minute readout of the ratiometric signal shows clear differences across varying concentrations of N6 fragment and provides enough time for the nanoparticles to reach a notable aggregation state. As such, the 10-minute mark is used as the standard for reporting the ratiometric signal in future assays. A control experiment using synthesized N-fragment (DADEFQLQ) incubated with BSPP-AuNPs was performed and no aggregation was observed due to the electrostatic repulsion between the negatively charged peptide and particles (Fig. S1†). Additionally, SV3CP alone incubated with BSPP-AuNPs showed no aggregation (Fig. S1†). High performance liquid chromatography (HPLC) and matrix-assisted laser desorption ionization–time-of-flight mass spectrometry (MALDI-TOF MS) (Fig. 2f and g) also confirm the cleavability of N6 and precision of the SV3CP cleavage by detection of the N6 N-terminal fragment.

## Zwitterionic peptide dynamic range optimization

The dynamic range of various peptide derivatives of N6 was examined to determine the optimal sequence for plasmonic sensing of SV3CP (Fig. 3). Table 2 details the sequences of the six peptides examined, along with their rationale. Computational folding data of each peptide is included in Fig. S2.† The dynamic range of each peptide is extracted by recording the ratiometric signal ($Abs_{600}/Abs_{520}$) at 10 minutes after addition of the BSPP-AuNPs (3.4 nM, 100 μL) to each peptide or pre-digested fragment at varying concentrations (*e.g.*, 0.1–100 μM). The lower limit of the dynamic range is determined by the critical coagulation concentration (CCC), the minimum concentration of peptide needed to induce coagulation of the AuNPs, of the pre-digested peptide while the upper limit is determined by the CCC of the intact peptide according to eqn (S1).† MALDI-TOF MS and HPLC confirmed the cleavability, or lack thereof, of each peptide (Fig. S3†).

In Fig. 3a, N3, a zwitterionic peptide containing two arginine units in addition to the lysine inherently found in the cleavage recognition site, induced a notable color change. Predigestion of N3 with SV3CP results in a slightly lower CCC due to the liberation of the charge-shielding site and +3 charged fragment, however, the overall dynamic range of the peptide is narrow: 2.9–7.2 μM. A peptide with a scramble of the cleavage sequence in N3, named N4, confirmed that cleavage of the substrate is required to segment the peptide into its charged fragments and induce a notable difference in plasmonic coupling, as noted by the over six-fold increase in the ratiometric signal, between the intact and fragmented peptide (Fig. 3b). Hence, N4 does not have a notable dynamic range, with both intact and SV3CP-incubated peptides having a similar effect as intact N3. Instead, the optimal sequence contains an aggregating site with a +2 charge when enzymatically cleaved. Specifically, our sequence, N6 (Fig. 3c) varies the positively charged residues containing one lysine and one arginine *versus* two arginine units. Variations in the amount of lysine units

were also examined (Fig. 3d and f), but were unable to aggregate the AuNPs or required high concentrations of fragmented peptide in the case of N7 (one lysine unit) and N9 (two lysine units) respectively. Additionally, the charge-shielding site is needed to establish a larger dynamic range, as omitting this sequence can result in a nearly three-fold reduction in the dynamic range as shown by N8 (Fig. 3e). Pre-digested N6 has a similar CCC as pre-digested N3, though the key difference lies in the CCC of the intact peptide, with the AuNPs retaining their colloidal stability in N6 concentrations of up to 100 μM. The resulting dynamic range has comparable sensitivity of the pre-digested peptide to our previously reported sequence but has a notably wider dynamic range.[9]

Our peptide design strategy shares some aspects discussed in prior work which used arginine, though lysine was not as thoroughly explored.[9,25,26] Increasing the amount of positively charged amino acids, arginine and/or lysine, results in the increasing charge valence of the liberated aggregating site and subsequent decrease in CCC, following similar trends summarized by the Schulz–Hardy rule.[25] Here, we report that additions of lysine units can result in more subtle changes of the CCC of AuNPs than arginine, as described by the behavior of N7 *versus* N6 or N9 (*e.g.*, N6's CCC is 2.0 μM whereas N9's CCC is 49.8 μM). This can be attributed to the difference in pH-dependent charge stability of the functional groups found in arginine and lysine, where the resonance-stabilized guanidine group in arginine makes it a strong baser than lysine's simple ammonium ion.[21–23] The resulting modulation of the CCC through a combination of arginine and lysine can fine tune the electrostatic peptide-induced AuNP aggregation, hence, there is a nearly two-fold increase in dynamic range of N6 over its arginine counterpart.[9]

## SV3CP detection and mechanistic study

We then used the optimal combination of N6 and BSPP-AuNPs to study our system's ability to detect SV3CP. Using a spectrophotometer, the limit of detection (LoD) for SV3CP was determined by eqn (S1)† to assess its clinical value. Based on the dynamic range of N6, a substrate concentration of 50 μM was used for all protein characterization studies. A minimum concentration of 2.0 μM of N6 is needed to aggregate the AuNPs, while the 50 μM of intact N6 should only slightly affect the colloidal stability of the particles. The enzyme assay was performed by incubating different concentrations of protease in TB-buffer with 50 μM of N6 in a 20 μL volume for 48 hours at 37 °C followed by subsequent addition of 100 μL AuNPs for a colorimetric readout. The clinically relevant concentration of SV3CP remains unclear, but our system achieves nanomolar sensitivity with a LoD of 28.0 nM (Fig. 4a). A shorter incubation time of 8 hours was also examined (Fig. S4a†), though it has a worse sensitivity with a LoD of 91.0 nM. This is an improvement over a previously reported FRET-based probe that showed a notable increase in signal starting at 250 nM.[27] As such, the standard incubation conditions for the subsequent assays reported uses 100 nM of SV3CP with a substrate incubation time of 48 hours at 37 °C. To further characterize the enzyme–substrate behavior of the custom substrate, a synthetic fluorogenic substrate, consisting of a similar peptide sequence conjugated to the 7-amino-4-methylcoumarin (AMC) fluorophore (Ac-EFQLQ-AMC) was used to determine the specificity constant ($k_{cat}/K_m$). For our substrate, a specificity constant of 739 $M^{-1}$ $s^{-1}$ was observed (Fig. 4b), which

is in good agreement with sequences reported in prior works developed for genogroup-1 (Southampton like) proteases.[27,28]

To test the specificity of our substrate to SV3CP, we cross-tested the effects of several related mammalian proteins on our sensing system including trypsin (*e.g.*, cleaves at the C-terminus of Arg or Lys), hemoglobin, salivary α-amylase (*e.g.* digests α-1,4-glucosidic bonds in starch),[29] thrombin (*e.g.*, cleaves the Arg-Gly bond in fibrinogen), and bovine serum albumin (BSA). Fig. 4c shows that only the positive control (*e.g.*, 100 nM SV3CP), yields a notable optical signal and subsequent colorimetric readout. While our substrate can be non-specifically cleaved by trypsin (DADEFQLQGK↓AR), the resulting +1 charged fragment (AR) is not sufficient to induce plasmonic coupling of the AuNPs, which agrees with our previous report.[25] This phenomenon was also demonstrated in the N7 peptide previously shown, where the subsequent C-fragment (GKAGGG) also carried a +1 charge and was unable to aggregate the particles (Fig. 3d). Fig. 4d gives additional insights into the enzyme-dependent activation of the colorimetric system. As a control, we heat-inactivated the protease by subjecting the SV3CP to high temperature conditions (60 °C, 3 hours) prior to substrate incubation. This is also intended to mimic the thermoregulatory immune response following infection.[30] As expected, heat treating SV3CP results in the denaturation and inactivation of the protease, suggesting a correlation between colloidal activity and the course of the infection.

Having established the system's dependency on the substrate-enzyme interaction, we then investigated the mechanism by which the charged peptide interacts with the BSPP-AuNPs to ensure that aggregation of the particles is indeed electrostatically induced. Reversibility experiments were conducted by employing several solvents and surfactants (10 mM) to better understand the interparticle interactions between N8/BSPP-AuNPs aggregates. In Fig. 4e, the gold pellet (3.4 nM, 100 μL), freshly clustered by N8 peptide (1.55 mM, 1 μL), readily dissociated and returned to a pinkish state in the presence of sodium dodecyl sulfate (SDS). Here, the excess anionic SDS scavenges the positively charged peptides and restores the electrostatic double layer repulsions between the particles.[31,32] NaOH also slightly redisperses the particles and can likely be attributed to the deprotonation of guanidium and ammonium ions at pH 11.0, restoring the electrostatic repulsions between nanoparticles.[7,9]

Lastly, we examine the performance of our system in various biological matrices relevant to HNV pathology and detection. Viral particles are primarily transmitted through aerosolized particles during vomiting and fecal matter contamination during diarrhea. Thus, release of SV3CP should theoretically occur in oral matrices such as saliva and exhaled breath and in stool samples for HNV-infected patients.[5,33,34] The colorimetric readout was determined in external breath condensate (EBC), 1% fecal matter, urine, 1% BSA, saliva, human plasma, and Dulbecco's modified Eagle's medium (DMEM) (Fig. 4f). BSPP-AuNPs were stable in all biological matrices except fecal matter, which required a minimum 1 in 5 dilution to avoid matrix-induced aggregation of the AuNPs (Fig. S4b†). The performance of our system in increasing dilutions of fecal matter is shown in Fig. S4c† which may be more clinically relevant to patient-derived samples due to the high-water content of diarrhea.[35] A 1 in 100 dilution is required to attain a notable colorimetric readout in fecal matter. This is likely attributed to the presence of complex polysaccharides found in fecal matter that

can non-specifically inhibit proteins—this is a known issue for RT-PCR based assays.[36] When spiked with SV3CP in the presence of the N6 peptide, AuNPs aggregated in EBC, 1% fecal matter, and urine. Additionally, more complex media such as BSA, saliva, human plasma, and cell culture medium largely impedes the aggregation of the nanoparticles, likely due to the abundance of negatively charged proteins forming a protein corona around the nanoparticles and/or scavenging the aggregating counterions.[7,37] Increasing dilution factors of these matrices, however, minimizes the aggregation impedance, as shown in a previous study.[6]

Overall, this approach offers a simple and intuitive alternative to conventional immunoassays that boasts label-free conditions without the need for complex laboratory equipment. Potential challenges in the detection of SV3CP using this approach include long substrate digestion times, nanomolar range detection limits, and potential false negatives in complex biological matrices (*e.g.* BSA, saliva, and plasma) due to the formation of protein coronas on the AuNPs. Our previous studies have adapted similar systems to diagnostic kits for face coverings and dipstick testing.[9,25,29] With remarkable specificity to SV3CP and functionality in select HNV-related biomatrices, this system can be used to non-invasively monitor HNV infections in the presence of >28.0 nM SV3CP (Fig. 4a) to complement existing detection portfolios.[38]

## Conclusions

An updated formula for zwitterionic peptides, $(Asp)_n(Glu)_o$-$(AA)_x$-$(Arg)_m(Lys)_p$ is reported to modulate the dispersity of BSPP-capped AuNPs and is applied to colorimetrically detect SV3CP, a key-protease implicated in the HNV viral lifecycle. Here, the novelty in this work is demonstrated through the choice of protease. We construct a label-free peptide (N6) in accordance with this formula, carrying a net −1 charge incapable of aggregating the negatively charged BSPP-AuNPs. Enzymatic cleavage of the peptide results in the liberation of a positively charged fragment, inducing plasmonic coupling between nanoparticles through electrostatic interactions. We quantified the color change using absorbance spectroscopy and showed the difference in aggregating propensity between arginine and lysine, providing optimizations of zwitterionic peptide design for colorimetric sensing. We then found the LoD of SV3CP in TB buffer to be 28.0 nM, with notable performance in EBC, 1% fecal matter, and urine using 100 nM of SV3CP. Cross-testing against other related mammalian proteins reveals no non-specific activation of the probe. Heat-denaturation of SV3CP confirms the critical role of enzymatic cleavage in mediating color change. The use of zwitterionic peptide/AuNP-based sensors does not require bioconjugation or sophisticated equipment, offering a promising solution for point-of-care qualitative diagnostics.

## Supplementary Material

Refer to Web version on PubMed Central for supplementary material.

## Acknowledgements

The authors acknowledge NIH funding under R01 DE031114.

## Data availability

The data that support the findings of this study are available from the corresponding author upon reasonable request.

## References


1. Lambden PR, Caul EO, Ashley CR and Clarke IN, Science, 1993, 259, 516–519. [PubMed: 8380940]
2. Hall AJ, Vinjé J, Lopman B, Park GW, Yen C, Gregoricus N and Parashar U, Morb. Mortal. Wkly. Rep.: Recomm. Rep, 2011, 60, 1–15.
3. Argudin MA, Mendoza MC and Rodicio MR, Toxins, 2010, 2, 1751–1773. [PubMed: 22069659]
4. Herod MR, Prince CA, Skilton RJ, Ward VK, Cooper JB and Clarke IN, Biochem. J, 2014, 464, 461–472. [PubMed: 25275273]
5. Capece G and Gignac E, in StatPearls, Treasure Island (FL), 2022, DOI: 10.1007/978-3-030-27209-8.
6. Zhou W, Gao X, Liu D and Chen X, Chem. Rev, 2015, 115, 10575–10636. [PubMed: 26114396]
7. Jin Z, Yeung J, Zhou J, Retout M, Yim W, Fajtová P, Gosselin B, Jabin I, Bruylants G, Mattoussi H, O'Donoghue AJ and Jokerst JV, ACS Appl. Mater. Interfaces, 2023, 15, 20483–20494. [PubMed: 37058597]
8. Jin Z, Yeung J, Zhou J, Cheng Y, Li Y, Mantri Y, He T, Yim W, Xu M, Wu Z, Fajtova P, Creyer MN, Moore C, Fu L, Penny WF, O'Donoghue AJ and Jokerst JV, Chem. Mater, 2022, 34, 1259–1268. [PubMed: 37406055]
9. Jin Z, Mantri Y, Retout M, Cheng Y, Zhou J, Jorns A, Fajtova P, Yim W, Moore C, Xu M, Creyer MN, Borum RM, Zhou J, Wu Z, He T, Penny WF, O'Donoghue AJ and Jokerst JV, Angew. Chem., Int. Ed, 2022, 61, e202112995.
10. Jin Z, Li Y, Li K, Zhou J, Yeung J, Ling C, Yim W, He T, Cheng Y, Xu M, Creyer MN, Chang Y-C, Fajtova P, Retout M, Qi B, Li S, O'Donoghue AJ and Jokerst JV, Angew. Chem, 2023, 135, e202214394.
11. De Graaf M, Van Beek J and Koopmans MPG, Nat. Rev. Microbiol, 2016, 14, 421–433. [PubMed: 27211790]
12. Bian T, Gardin A, Gemen J, Houben L, Perego C, Lee B, Elad N, Chu Z, Pavan GM and Klajn R, Nat. Chem, 2021, 13, 940–949. [PubMed: 34489564]
13. Sener G, Uzun L and Denizli A, ACS Appl. Mater. Interfaces, 2014, 6, 18395–18400. [PubMed: 25330256]
14. Guarise C, Pasquato L, De Filippis V and Scrimin P, Proc. Natl. Acad. Sci. U. S. A, 2006, 103, 3978–3982. [PubMed: 16537471]
15. Chen J, Ma Y, Du W, Dai T, Wang Y, Jiang W, Wan Y, Wang Y, Liang G and Wang G, Adv. Funct. Mater, 2020, 30, 2001566.
16. Retout M, Jin Z, Tsujimoto J, Mantri Y, Borum R, Creyer MN, Yim W, He T, Chang YC and Jokerst JV, ACS Appl. Mater. Interfaces, 2022, 14, 52553–52565. [PubMed: 36346346]
17. Guo J, Douangamath A, Song W, Coker AR, Chan AWE, Wood SP, Cooper JB, Resnick E, London N and Delft F. v., J. Struct. Biol.: X, 2020, 4, 100031. [PubMed: 32743543]
18. Mei BC, Oh E, Susumu K, Farrell D, Mountziaris TJ and Mattoussi H, Langmuir, 2009, 25, 10604–10611. [PubMed: 19588955]
19. Jin Z, Sugiyama Y, Zhang C, Palui G, Xin Y, Du L, Wang S, Dridi N and Mattoussi H, Chem. Mater, 2020, 32, 7469–7483.
20. Yon M, Pibourret C, Marty JD and Ciuculescu-Pradines D, Nanoscale Adv, 2020, 2, 4671–4681. [PubMed: 36132884]
21. Vazdar M, Heyda J, Mason PE, Tesei G, Allolio C, Lund M and Jungwirth P, Acc. Chem. Res, 2018, 51, 1455–1464. [PubMed: 29799185]

22. Dardonville C, Caine BA, Navarro De La Fuente M, Herranz GM, Mariblanca BC and Popelier PLA, New J. Chem, 2017, 41, 11016–11028.
23. André I, Linse S and Mulder FAA, J. Am. Chem. Soc, 2007, 129, 15805–15813. [PubMed: 18044888]
24. Cutrona KJ, Kaufman BA, Figueroa DM and Elmore DE, FEBS Lett, 2015, 589, 3915–3920. [PubMed: 26555191]
25. Chang YC, Jin Z, Li K, Zhou J, Yim W, Yeung J, Cheng Y, Retout M, Creyer MN, Fajtova P, He T, Chen X, O'Donoghue AJ and Jokerst JV, Chem. Sci, 2023, 14, 2659–2668. [PubMed: 36908948]
26. Jin Z, Ling C, Li Y, Zhou J, Li K, Yim W, Yeung J, Chang YC, He T, Cheng Y, Fajtová P, Retout M, O'Donoghue AJ and Jokerst JV, Nano Lett, 2022, 22, 8932–8940. [PubMed: 36346642]
27. Viswanathan P, May J, Uhm S, Yon C and Korba B, Virology, 2013, 438, 20–27. [PubMed: 23399036]
28. Chang KO, Takahashi D, Prakash O and Kim Y, Virology, 2012, 423, 125–133. [PubMed: 22200497]
29. Jin Z, Jorns A, Yim W, Wing R, Mantri Y, Zhou J, Zhou J, Wu Z, Moore C, Penny WF and Jokerst JV, Anal. Chem, 2021, 93, 11025–11032. [PubMed: 34309356]
30. Hellysaz A, Neijd M, Vesikari T, Svensson L and Hagbom M, mBio, 2023, 14, e03567–22. [PubMed: 36976000]
31. Jung JM, Savin G, Pouzot M, Schmitt C and Mezzenga R, Biomacromolecules, 2008, 9, 2477–2486. [PubMed: 18698816]
32. Wu D, Zhou J, Creyer MN, Yim W, Chen Z, Messersmith PB and Jokerst JV, Chem. Soc. Rev, 2021, 50,4432–4483. [PubMed: 33595004]
33. Tung-Thompson G, Libera DA, Koch KL, De Los Reyes FL and Jaykus LA, PLoS One, 2015, 10, e0134277. [PubMed: 26287612]
34. Colquhoun DR, Schwab KJ, Cole RN and Halden RU, Appl. Environ. Microbiol, 2006, 72, 2749. [PubMed: 16597979]
35. Nemeth V and Pfleghaar N, in StatPearls, Treasure Island (FL), 2023.
36. Monteiro L, Bonnemaison D, Vekris A, Petry KG, Bonnet J, Vidal R, Cabrita J and Megraud F, J. Clin. Microbiol, 1997, 35, 995–998. [PubMed: 9157172]
37. Rampado R, Crotti S, Caliceti P, Pucciarelli S and Agostini M, Front. Bioeng. Biotechnol, 2020, 8,166. [PubMed: 32309278]
38. Vinjé J, J. Clin. Microbiol, 2015, 53, 373–381. [PubMed: 24989606]

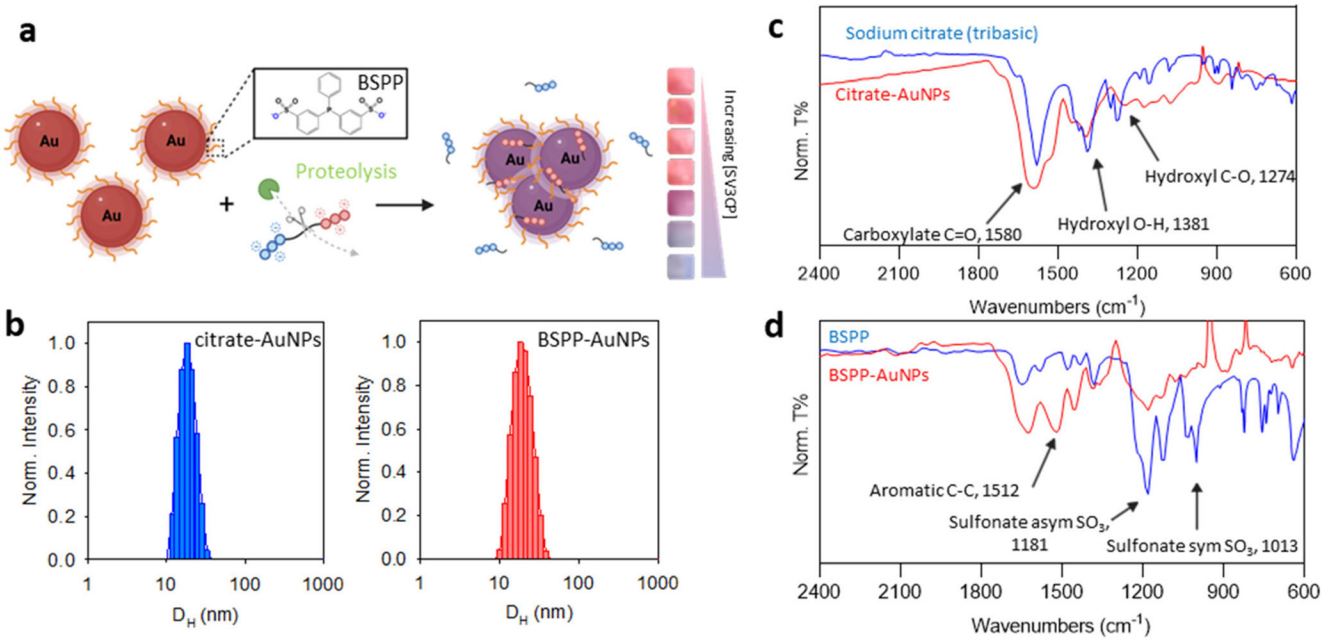


**Fig. 1.**

Mechanism of the plasmonic sensing system and characterization of the citrate-AuNP to BSPP-AuNP ligand exchange. (a) Schematic illustration of plasmonic sensing using BSPP-AuNPs. The green cartoon represents SV3CP; red and blue circles represent the positively and negatively charged amino acids, respectively, flanking the cleavage site. (b) DLS profiles of citrate-AuNPs (blue) and BSPP-AuNPs (red). FTIR spectra over the range of 2400–600 $cm^{-1}$ of (c) citrate-AuNPs and (d) BSPP-AuNPs. The C═O signatures are associated with the carboxylate groups in sodium citrate, while the aromatic C–C and S–O signatures are from BSPP. This is indicative of a successful ligand exchange to make the BSPP-AuNPs.

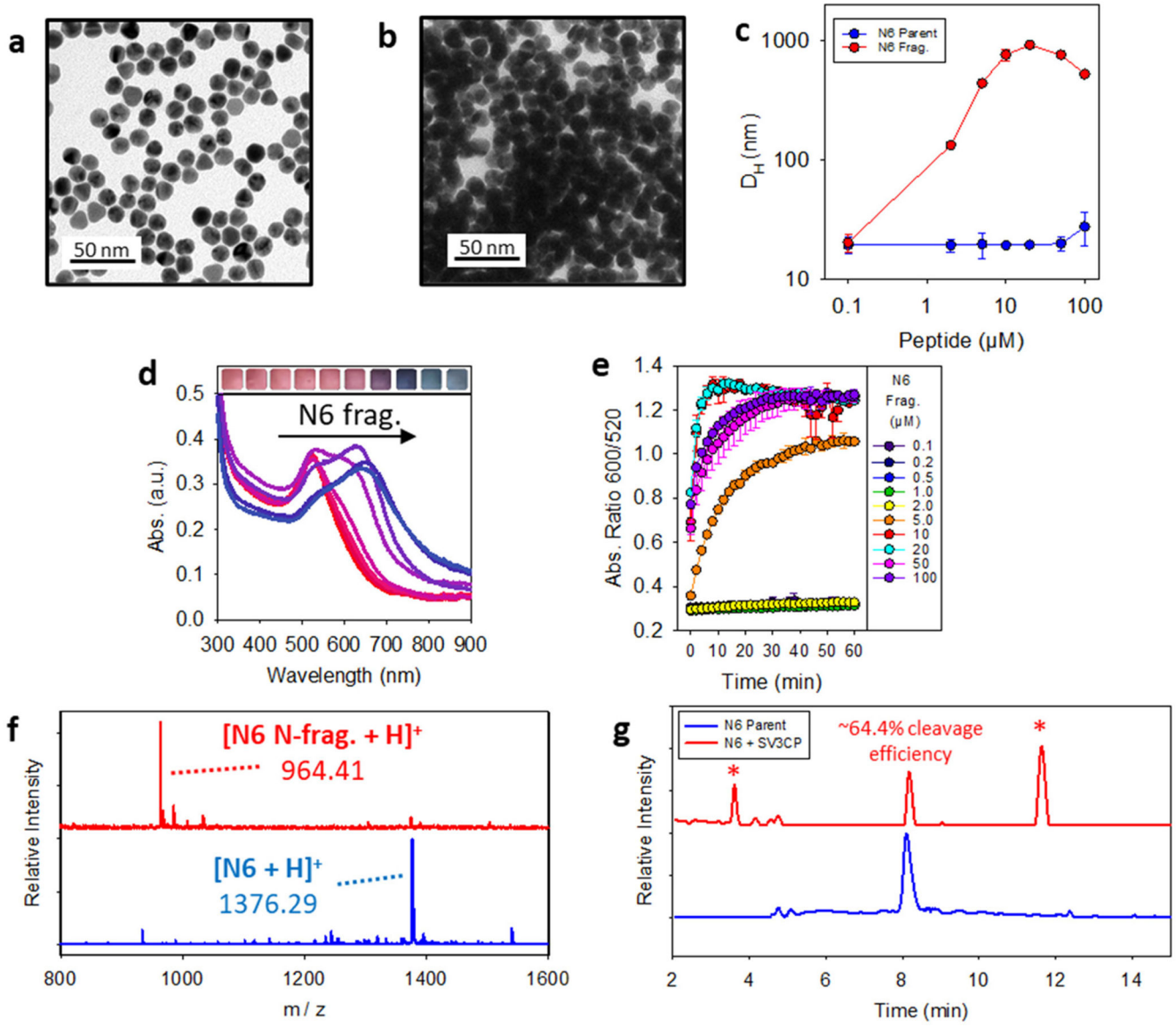


**Fig. 2.**

Characterization of AuNP aggregates with N6 fragments pre-cleaved by SV3CP. TEM images of the BSPP-AuNPs when incubated with (a) intact N6 and (b) SV3CP-cleaved N6 fragments. (c) DLS profiles of BSPP-AuNPs incubated with increasing concentrations of intact (blue) and SV3CP-cleaved (red) N6 peptide. No change was seen in the hydrodynamic diameter (DH) in the particles with the intact peptide whereas a sizable change is seen when incubated with N6 fragments of at least ~2 μM. (d) Optical absorption and color visuals of BSPP-AuNPs (3.4 nM, 100 μL with increasing concentrations of N6 fragments. The arrow denotes the absorption band shift and corresponding color evolution. (e) Kinetic measurements of the ratiometric signal, $Abs_{600}/Abs_{520}$, were taken over 60 minutes for increasing concentrations of N6 fragments (*e.g.*, 0.1, 0.2, 0.5, 1, 2, 5, 10, 20, 50, and 100 μM). The 10-minute readout showed a notable change in the ratiometric signal, which plateaus after 60 minutes. Error bars = standard deviation ($n$ = 3). (f) HPLC of N6 before

and after incubation with SV3CP. '*' denotes the presence of new peaks due to proteolysis. N6 was incubated with SV3CP at a [E] : [S] ratio of 1 : 200 for 48 hours, resulting in a 64.4% cleavage efficiency. (g) MALDI-TOF mass spectrometry of N6 peptide before (blue) and after (red) incubation with SV3CP. Proteolysis is confirmed through the detection of the N6 N-fragment. Analysis of the cleavage was conducted on the crude proteolysis reaction; mass spectrometry of individual HPLC peaks was not suitable because the fractions had low yields.

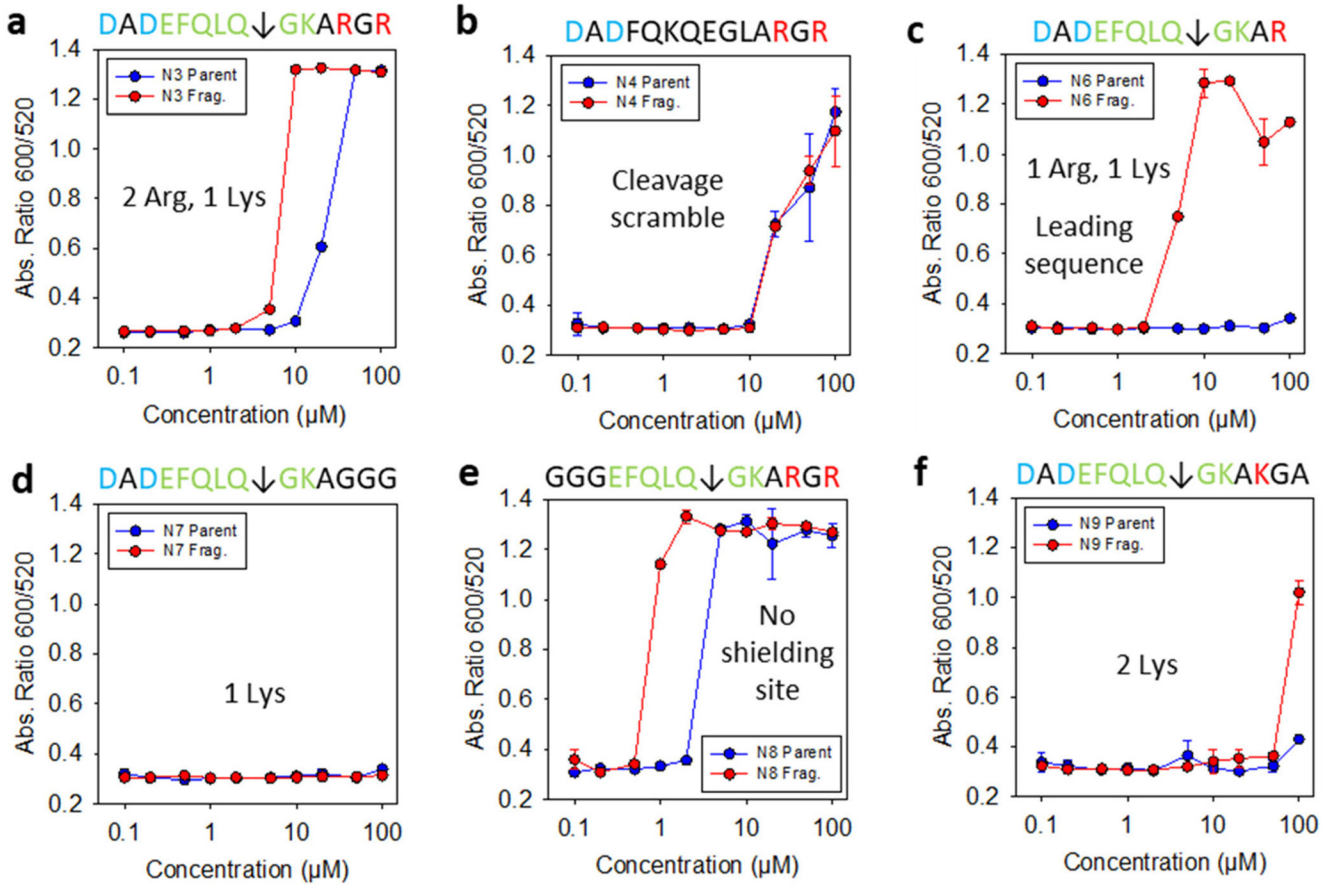


**Fig. 3.**

Dynamic range of peptides. Ratiometric signal ($Abs_{600}/Abs_{520}$ at 10 min) was recorded from BSPP-AuNPs when incubated with various amounts of (a) N3, (b) N4, (c) N6, (d) N7, (e) N8, and (f) N9 intact (blue) and SV3CP-cleaved (red) peptides. Amino acids units labeled in blue, green, and red correspond with charge-shielding, cleavage recognition, and aggregation respectively. Increasing additions of Lys and/or Arg result in lower detection limits in both the intact and fragmented peptides. This broadly follows the trends outlined in a peptide valence study based on the Schulz–Hardy rule.[23] Error bars = standard deviation ($n = 3$).

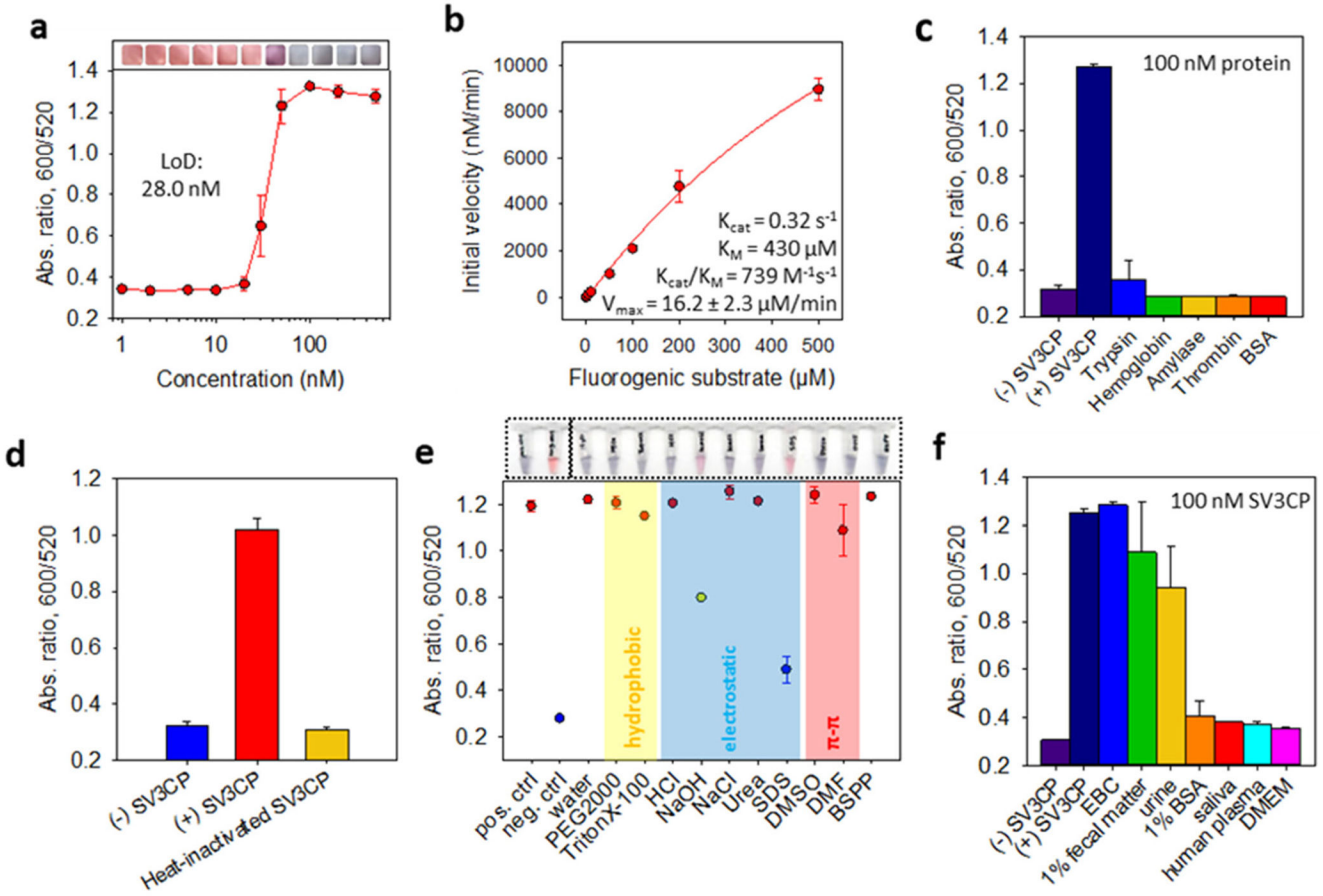


**Fig. 4.**

Sensitivity and specificity testing and sensing mechanism exploration. (a) Ratiometric absorbance as a function of SV3CP concentration, with color visuals on top. N6 substrate and BSPP-AuNPs (3.4 nM) were employed. The substrate was incubated with the protease in TB buffer for 48 hours before addition of BSPP-AuNPs. (b) $k_{cat}/K_m$ determination of the hydrolysis of fluorogenic substrate (*Ac*-EFQLQ-*AMC*) by SV3CP in 0.02M TB buffer, NaCl 150 mM, 5 mM DTT, pH 8.0. SV3CP (850 nM) was incubated with varying fluorogenic substrate concentrations (*e.g.*, 0.1–500 μM). Data was fitted to the Michaelis–Menten equation (eqn (S3)†). (c) System interferance by other mammalian proteins (100 nM) in TB buffer, including trypsin, hemoglobin, amylase, thrombin, and BSA. Samples with and without SV3CP served as positive and negative controls, respectively. (d) Thermoregulated heat inactivation of SV3CP (100 nM). SV3CP was heated at 60 °C for 3 hours prior to substrate incubation for 48 hours. The resulting colorimetric readout shows the system's dependence on SV3CP-activity. (e) White-light image (top) and quantified reversal of color change (bottom). Redispersion in SDS indicates dominant electrostatic forces. (f) System performance in biological matrices. The positive control used 100 nM of SV3CP in buffer and the negative control is buffer without SV3CP. Error bars = standard deviation ($n$ = 3).

**Table 1**

Hydrodynamic size and zeta potential of citrate-AuNPs and BSPP-AuNPs

| Sample | DLS: $D_H$ (nm) | DLS: PDI | Zeta: ζ (mV) |
|---|---|---|---|
| Citrate-AuNPs | 18.9 | 0.22 | −29.8 ± 2.4 |
| BSPP-AuNPs | 19.9 | 0.23 | −31.0 ± 1.4 |

**Table 2**

Peptide information (*e.g.*, $(Asp)_n(Glu)_o$-$(AA)_x$-$(Arg)_m(Lys)_p$) and operating windows

| Peptide name | Sequence | M. W. (g $mol^{-1}$) | Net charge[a] | Dynamic range[b] (μM) | Rationale |
|---|---|---|---|---|---|
| N3 | DADEFQLQ↓GKARGR | 1588.8 | 0 | 2.9–7.2 | Single lysine, double arginine |
| N4 | DADFQKQEGLARGR | 1588.8 | 0 | — | Cleavage scramble |
| N6 | DADEFQLQ↓GKAR | 1375.7 | −1 | 2.0–100.0 | Single lysine, single arginine; leading sequence |
| N7 | DADEFQLQ↓GKAGGG | 1390.6 | −2 | — | Single lysine; minimized aggregating site |
| N8 | GGGEFQLQ↓GKARGR | 1458.8 | +2 | 0.3–1.9 | No shielding site |
| N9 | DADEFQLQ↓GKAKGA | 1475.7 | −1 | 49.8–100.0 | Double lysine |

[a]The electrophoretic property at pH 8.0; note that all peptides contain a free N-terminus (*e.g.*, –NH2 uncharged at pH 8.0) and an amidated C-terminus (*e.g.*, –Am).

[b]The dynamic range of each peptide was determined in Tris-buffer (TB) containing 150 mM NaCl and 5 mM DTT at pH 8.